

Fluorescence Relaxation Dynamics of Acridine Orange in Nanosized Micellar Systems and DNA

Ajay Kumar Shaw and Samir Kumar Pal*

Unit for Nanoscience and Technology, Department of Chemical, Biological, and Macromolecular Sciences, Satyendra Nath Bose National Centre for Basic Sciences, Block JD, Sector III, Salt Lake, Kolkata 700 098, India

Received: October 31, 2006; In Final Form: February 3, 2007

In this paper, we report a detailed study of the fluorescence relaxation dynamics of a well-known fluorescent DNA intercalator, acridine orange (AO), in reverse micelles (RM), micelles, and DNA using picosecond resolved fluorescence spectroscopy. Solvation studies of AO in AOT reverse micelles (RM) containing water indicate the locations of AO close to the interface and those in RM containing NaOH; there are two types of AO—one in the nonpolar oil phase and the other at the interface. The bound water at the reverse micellar interface is found to be much more rigid than that at the micellar interface of sodium dodecyl sulfate (SDS) micelles. Dynamic light scattering (DLS) studies allow for the determination of the hydrodynamic radius and the overall tumbling motion of the macromolecules. Wobbling-in-cone data analysis of the temporal fluorescence anisotropy decay allows for determination of restriction on the motion of fluorophores attached to the macromolecules. This model further applied to AO-intercalated genomic DNA and synthetic oligonucleotides within their structural integrity (as confirmed through circular dichroism (CD) studies) shows that AO experiences less restriction in genomic salmon sperm DNA compared with that in synthetic oligonucleotides, and among the oligonucleotides, the ones with AT base pairs are much more rigid. This study would invoke further research on the dynamical nature of AO in restricted environments.

Introduction

The interactions of small molecules with normal and inverted micelles have been a subject of very extensive study.^{1–5} Micelles are aggregates of surfactant (amphiphilic) molecules, which are formed above a certain critical concentration of monomeric surfactant molecules. These interactions include a wide range of studies, *viz.*, (1) solubilization of various types of solutes, (2) solute–micelle complexation, (3) changes in micellar properties due to incorporation of solute, and (4) the effects of micelles on the thermodynamics and kinetics of processes taking place in these systems. Reverse micelles (RMs) are nanopools of polar solvent protected by a monolayer of surfactant molecules at the periphery with polar head groups pointing inward toward the polar solvent, and the hydrocarbon tails are directed toward the nonpolar organic solvents.^{4,6} The chemical approach to biological problems through investigations of models rests upon the ability of the chosen system to mimic some functions of biological ensembles. RMs with water nanopools resemble the water pockets found in various bioaggregates such as proteins, membranes, and mitochondria. Thus, these systems are very often considered as excellent biomimics for exploration of biological membranes and biologically confined water molecules.^{7–10}

The aerosol–OT(AOT)–alkane–water system is interesting as the solution is homogeneous and optically transparent over a wide range of temperature, pressure, and pH. The AOT RM can compartmentalize a large amount of water in its central core, and the nanoscale aggregation process is fairly well characterized with respect to size and shape at various water contents.¹¹ RMs are well-known as common organic media to perform bio-

analysis. They have been associated with the idea of a “Nano-Cage” or “Micro-Reactor”.^{4,12,13} Aqueous RMs are generally characterized by the hydration parameter w_0 , which is the ratio of molar concentration of water to that of surfactant. RMs with w_0 values less than 20 are stable and monodisperse over a wide range of temperatures.⁴ In liquid alkanes, AOT RMs ($w_0 = 0$) are completely associated and each micelle contains 23 monomers. The structures of these RMs are slightly asymmetric and are of round cylindrical nature.¹¹ The structures of AOT RMs have been extensively studied using several methods such as ¹H NMR,^{14–16} IR,^{17–20} ESR (electron spin resonance),²¹ photon correlation spectroscopy,^{22,23} SANS (small-angle neutron scattering),^{24,25} dielectric studies,^{26,27} and molecular dynamics simulations.²⁸ Fluorescence spectroscopy has also been extensively used to study the AOT RM system. Fluorescent probes have been used to determine the viscosity, binding site, rigidity, and proximity within the water pool.^{29–33} Fluorescence has also been used to study the excited-state proton transfer inside the AOT RM(s),^{10,34–39} which has attracted considerable attention due to its extensive role in biological and chemical phenomena.

These studies have shown that water inside the RM is generally of two types: (i) interfacial (bound) and (ii) core (free) water. One of the studies¹⁷ has shown the existence of a third type of water (trapped) molecule present between the polar head groups of the individual surfactant molecules. Thus, the interior of RMs is extremely heterogeneous, and a polar fluorescent probe has a finite possibility of distribution in any of these regions. Because there is wide difference in rigidity of the interfacial and core water molecules, the solvent relaxation around the excited probe molecule is expectedly multiexponential. Various fluorescent probes, betaine,^{40,41} ANS,⁴² ethidium bromide,⁴³ and acridine derivatives,^{44–47} have been used to study the interior of RMs. Acridine orange (AO), a cationic dye, is a

* Corresponding author. E-mail: skpal@bose.res.in. Fax: 91 33 2335 3477.

well-known DNA intercalator^{48–50} and is useful for studying the photophysics and molecular dynamics of DNA.^{51,52} Acridine dyes were widely used as antibacterial and antimalarial drugs during World War II.⁵³ AO is known to form dimers at higher concentrations,^{54,55} and Stark effect spectroscopy⁵⁶ has been used for assessment of electronic coupling in dimeric structures of AO. AO is also used as biological stains in fluorescence microscopy⁵⁷ and finds wide usage in photodynamic therapy.^{58,59} In recent reports, few groups have studied the interactions of AO (both protonated and deprotonated) with anionic surfactant aggregates in order to investigate the aqueous environment of RM^{44,45} and also to explore the proton-transfer photophysics of AO inside the RM. Diffusional dynamics of AO in SDS⁶⁰ and at the liquid alkane–water⁶¹ interface have also been studied. Very recently, from our group, the homomolecular fluorescence resonance energy transfer properties of AO⁶² have been used to show that genomic DNA assumes polymer and salt-induced (psi) condensed forms⁶³ inside anionic AOT RMs. In this report, we have studied in detail the solvation and fluorescence depolarization dynamics of AO in AOT RMs containing water (pH = 6.9) and NaOH (pH = 13.6), SDS, CTAB, and TX100 normal micelles using picosecond time-resolved fluorescence spectroscopy. We have also applied a wobbling-in-cone model to analyze and interpret the time-resolved fluorescence anisotropy decay data of AO in these restricted environments. We have further applied this model to AO intercalated inside genomic salmon sperm DNA and two synthetic oligonucleotides: (1) (GCGCGCGCGCGC)₂ (oligo1) and (2) (CGCAAATTTGCG)₂ (oligo2) to study the reorientational dynamics of the probe AO within the intercalation site and thus to predict the rigidity of genomic DNA and synthetic oligonucleotides.

Materials and Methods

Sample Preparation. Acridine orange (AO), DNA (from salmon testes; SS-DNA), bis(2-ethylhexyl)sulfosuccinate (AOT), cetyltrimethyl ammonium bromide (CTAB), sodium dodecyl sulfate (SDS), and TritonX-100 (TX100) were purchased from Sigma and Fluka and used as received. Isooctane was purchased from Spectrochem. The purified (reverse phase cartridge) synthetic DNA oligonucleotides of 12 bases (dodecamer) with sequences GCGCGCGCGCGC and CGCAAATTTGCG were obtained from Gene Link. In order to reassociate the single strand DNA into self-complementary ds-DNA (GCGCGCGCGCGC)₂ (oligo1) and (CGCAAATTTGCG)₂ (oligo2), thermal annealing was performed as per the methodology prescribed by the vendor. The aqueous solutions of the oligonucleotides were dialyzed exhaustively against Millipore water prior to further use. The procedure for making genomic DNA aqueous solutions is similar to that as mentioned in the earlier studies.^{64,65} In the present study, the concentration of DNA base pairs (bp) is considered the overall concentration of the DNA. The nucleotide concentrations were determined by absorption spectroscopy using the average extinction coefficient per nucleotide of the DNA (6600 M⁻¹ cm⁻¹ at 260 nm)⁶⁵ and found to be 4.23 (SS-DNA), 5.16 (oligo1), and 4.08 mM (oligo2). For spectroscopic studies, the AO–DNA complex with a [AO]:[DNA] ratio of 1:100 was prepared by adding dropwise a calculated volume of known concentrated AO solution into a given volume of known concentrated DNA solution with continuous stirring for 2 h. The RM solutions of AO were prepared by adding requisite volumes of AO solution into a given volume of 100 mM AOT solution in isooctane with vigorous stirring to achieve RMs with various w_0 values. The overall concentration of AO for different w_0 values in RM solutions containing water or NaOH was kept

fixed. However, in all the experiments, the concentrations of micelles were much higher than that of AO to ensure that not more than one AO is held by one micelle.

Steady-State Study. Steady-state absorption and emission were measured with a Shimadzu Model UV-2450 spectrophotometer and a Jobin Yvon Model Fluoromax-3 fluorimeter, respectively. Circular dichroism (CD) studies were done using a Jasco 810 spectropolarimeter with a quartz cell of 2 mm optical path length. Dynamic light scattering (DLS) measurements were done with Nano S Malvern instruments employing a 4 mW He–Ne laser ($\lambda = 632.8$ nm) and equipped with a thermostatted sample chamber. All the scattered photons were collected at a 173° scattering angle at 298 K. The scattering intensity data were processed using the instrumental software to obtain the hydrodynamic diameter (d_H) and the size distribution of the scatterer in each sample. The instrument measures the time-dependent fluctuation in intensity of light scattered from the particles in solution at a fixed scattering angle. Hydrodynamic diameters (d_H) of the particles were estimated from the intensity auto-correlation function of the time-dependent fluctuation in intensity. d_H is defined as

$$d_H = \frac{k_B T}{3\pi\eta D} \quad (1)$$

where k_B is the Boltzmann constant, T the absolute temperature, η the viscosity, and D the translational diffusion coefficient. In a typical size distribution graph from the DLS measurement, the X -axis shows a distribution of size classes in nanometers, and the Y -axis shows the relative intensity of the scattered light. This is therefore known as an intensity distribution graph.

Time-Resolved Study. All fluorescence decays were taken by using the picosecond-resolved time-correlated single-photon counting (TCSPC) technique. The commercially available setup is a picosecond diode laser pumped time-resolved fluorescence spectrophotometer from Edinburgh Instrument (LifeSpec-ps), U.K. The picosecond excitation pulse from the Picoquant diode laser was used at 375 nm. A liquid scatterer was used to measure the FWHM of the instrument response functions (IRF). It has an instrument response function (IRF) of 80 ps. Fluorescence photons from the sample were detected by a microchannel plate photo multiplier tube (MCP-PMT, Hammamatsu) after dispersion through a grating monochromator. For all decays, the emission polarizer was set at 54.7° (magic angle) with respect to the polarization axis of the excitation beam.

Methods of Data Analysis. The observed fluorescence transients are fitted by using a nonlinear least-square fitting procedure (software supplied by Edinburgh Instruments) to a function ($X(t) = \int_0^t E(t')R(t-t') dt'$) comprising convolution of the IRF ($E(t)$) with a sum of exponentials ($R(t) = A + \sum_{i=1}^N B_i e^{-t/\tau_i}$) with preexponential factors (B_i), characteristic lifetimes (τ_i), and a background (A). Relative concentration in a multiexponential decay is finally expressed as $\tau_n = \tau_n B_n / \sum_{i=1}^N B_i \tau_i \times 100$. The quality of the curve fitting was evaluated by reduced chi-square (0.90–1.09) and residual data. The purpose of the fitting is to obtain the decays in an analytic form suitable for further data analysis.

To construct time-resolved emission spectra (TRES), we followed the technique described in refs 66 and 67. As described above, the emission intensity decays are analyzed in terms of the multiexponential model,

$$I(\lambda, t) = \sum_{i=1}^N \alpha_i(\lambda) \exp[-t/\tau_i(\lambda)] \quad (2)$$

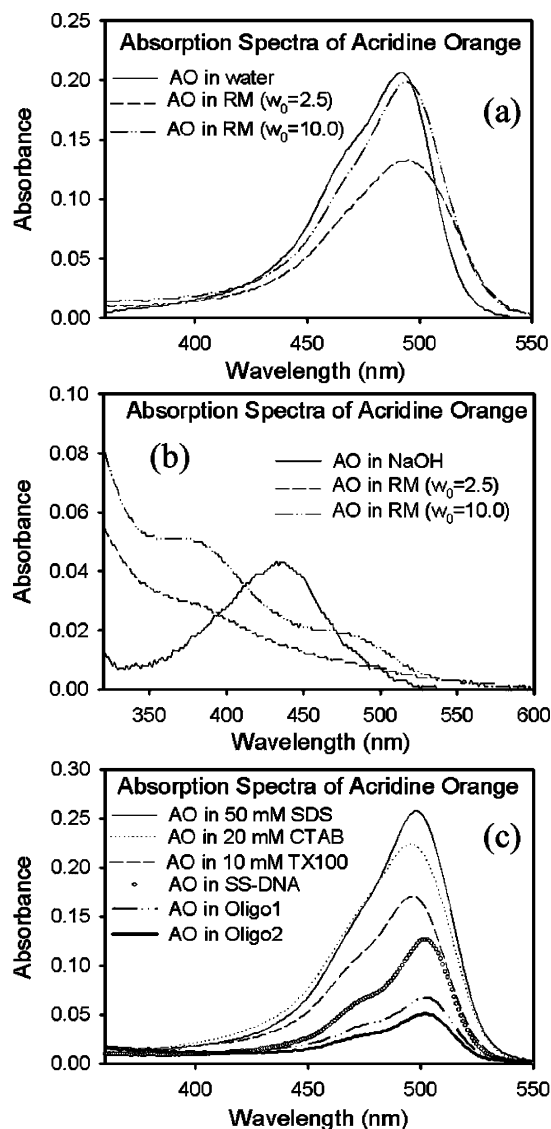


Figure 1. Absorption spectra of acridine orange (AO) in (a) RMs containing water, (b) RMs containing NaOH, and (c) micelles (SDS, CTAB and TX100) and DNA (salmon sperm, oligo1, and oligo2).

where $\alpha_i(\lambda)$ are the preexponential factors, with $\sum \alpha_i(\lambda) = 1.0$. In this analysis, we compute a new set of intensity decays, which are normalized so that the time-integrated intensity at each wavelength is equal to the steady-state intensity at that wavelength. Considering $F(\lambda)$ to be the steady-state emission spectrum, we calculated a set of $H(\lambda)$ values using

$$H(\lambda) = \frac{F(\lambda)}{\int_0^{\infty} I(\lambda, t) dt} \quad (3)$$

which for multiexponential analysis becomes

$$H(\lambda) = \frac{F(\lambda)}{\sum_i \alpha_i(\lambda) \tau_i(\lambda)} \quad (4)$$

Then, the appropriately normalized intensity decay functions are given by

$$I'(\lambda, t) = H(\lambda) I(\lambda, t) = \sum_{i=1}^N \alpha'_i(\lambda) \exp[-t/\tau_i(\lambda)] \quad (5)$$

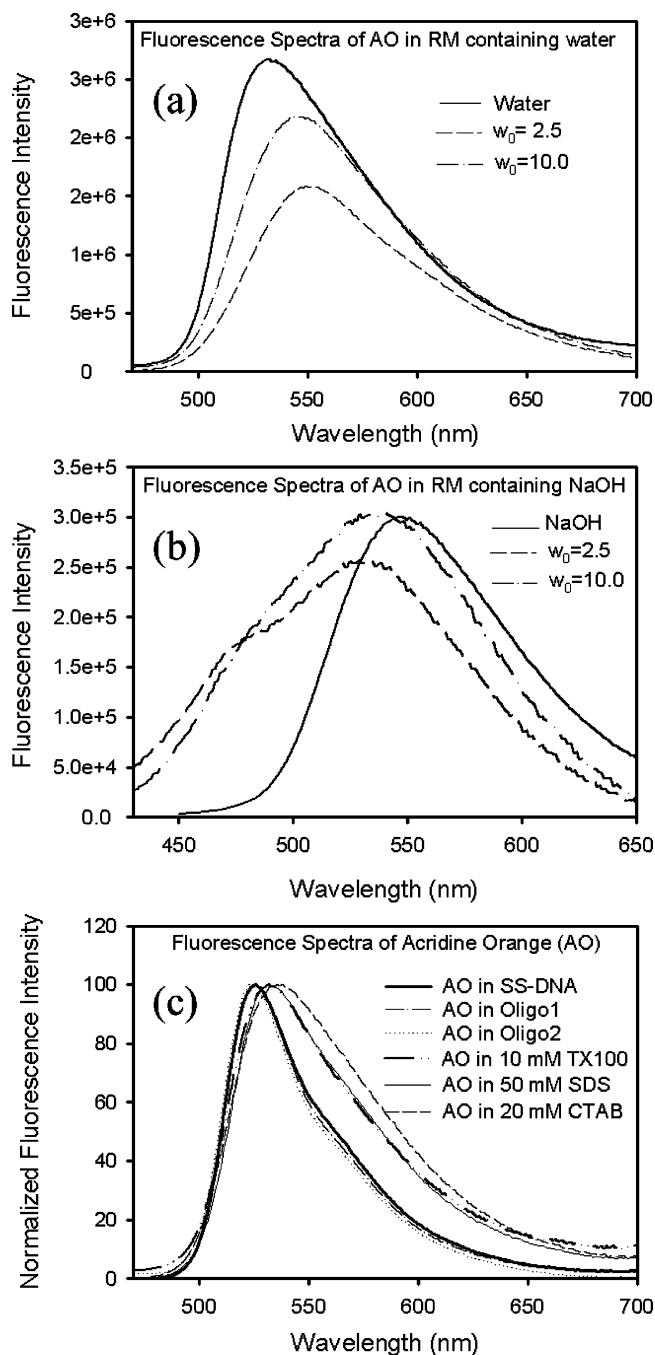
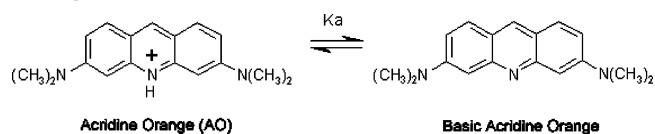


Figure 2. Fluorescence spectra of acridine orange (AO) in (a) RMs containing water, (b) RMs containing NaOH, and (c) micelles (SDS, CTAB, and TX100) and DNA (salmon sperm, oligo1, and oligo2).

SCHEME 1: Acid–Base Equilibrium of Acridine Orange



where $\alpha'_i(\lambda) = H(\lambda) \alpha_i(\lambda)$. The values of $I'(\lambda, t)$ are used to calculate the intensity at any wavelength and time and thus the TRES. The values of the emission maxima and spectral width are determined by nonlinear least-square fitting of the spectral shape of the TRES. The spectral shape is assumed to follow a log-normal line shape,⁶⁶

$$I(\bar{\nu}) = I_0 \exp \left\{ - \left[\ln 2 \left(\frac{\ln(\alpha + 1)}{b} \right)^2 \right] \right\} \quad (6)$$

with $\alpha = (2b(\bar{\nu} - \bar{\nu}_{\max}))/b - 1$, where I_0 is amplitude, $\bar{\nu}_{\max}$ is the wavenumber of the emission maximum, and spectral width is given by

$$\Gamma = \Delta \left[\frac{\sinh(b)}{b} \right]$$

where the terms Δ and b are width and asymmetry parameters, respectively. Equation 6 reduces to a Gaussian function for $b = 0$. The TRES thus obtained are used to construct the solvation correlation function $C(t)$ as

$$C(t) = \frac{\nu(t) - \nu(\infty)}{\nu(0) - \nu(\infty)} \quad (7)$$

where $\nu(0)$, $\nu(t)$, and $\nu(\infty)$ are the frequencies of emission maxima at times 0, t , and ∞ , respectively. The $C(t)$ curves thus obtained represent the solvent relaxation dynamics around the excited probe molecule.

We have also constructed the time-resolved area normalized emission spectrum (TRANES) to determine the kind of species present in the system and the environment about the species.^{68–70} TRANES is a model free modified version of TRES as mentioned above. A useful feature of the method is that an isoemissive point in the spectra involves two emitting species, which are kinetically coupled either irreversibly or reversibly or not coupled at all. In the recent literature, various other groups^{71,72} have also used the TRANES technique to confirm two emissive species in the micro-heterogeneous environments. For all anisotropy measurements, the emission polarizer was adjusted parallel and perpendicular to that of the excitation polarizer and the anisotropy is defined⁶⁷ as

$$r(t) = \frac{I_{\parallel}(t) - GI_{\perp}(t)}{I_{\parallel}(t) + 2GI_{\perp}(t)} \quad (8)$$

where $I_{\parallel}(t)$ and $I_{\perp}(t)$ are the temporal emission intensities at parallel and perpendicular emission polarization with respect to vertical excitation polarization. G is the correction factor of the polarization bias of the detection setup. The G factor at a given wavelength was independently obtained by exciting the sample with a horizontally polarized excitation beam and collecting the two polarized fluorescence decays, one parallel and other parallel to the horizontally polarized excitation beam. The $r(t)$ was fitted biexponentially as follows:

$$r(t) = r_0[\alpha_1 e^{-t/\phi_1} + \alpha_2 e^{-t/\phi_2}] \quad (9)$$

where ϕ_1 and ϕ_2 are the two rotational correlation time constants and α_1 and α_2 are the corresponding amplitudes. r_0 is the limiting anisotropy that describes the inherent depolarization of a given molecule.

Wobbling-in-Cone Model. The biexponential anisotropy decay can be analyzed using the two-step and wobbling-in-cone model.^{73,74} According to this model, the observed slow rotational relaxation with larger rotational time constants (τ_s) is described as a convolution of lateral diffusional relaxation with a time constant τ_L of the probe along the micellar interface and the overall tumbling motion of the micelle with time constant τ_M .⁷⁵

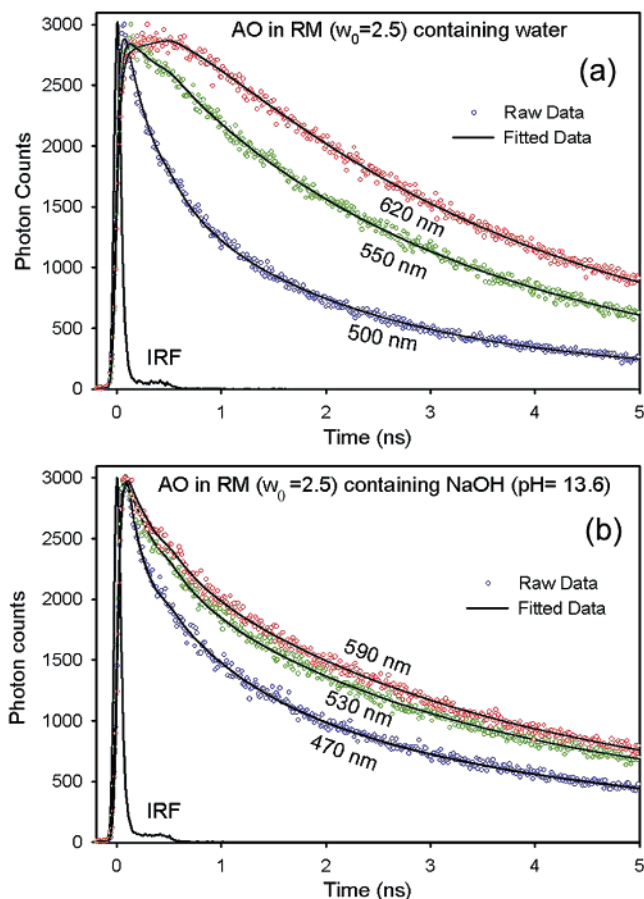


Figure 3. Fluorescence decay transients at various wavelengths of AO in RMs ($w_0 = 2.5$) containing (a) water and (b) NaOH.

TABLE 1: Steady-State Absorption and Fluorescence Data of Acridine Orange in Various Environments

systems	absorption peak (nm)	fluorescence peak (nm)
water (pH = 6.9)	492	532
NaOH (pH = 13.6)	435	546
RMs with water ($w_0 = 2.5$)	495	549
RMs with water ($w_0 = 10.0$)	494	545
RMs with NaOH ($w_0 = 2.5$)	375, 460	470, 533
RMs with NaOH ($w_0 = 10.0$)	375, 460	477, 538
20 mM CTAB	496	536
50 mM SDS	498	531
10 mM TX100	496	532
SS-DNA	502	526
(GCGCGCGCGCG) ₂ (oligo1)	502	526
(CGCAAATTTGCG) ₂ (oligo2)	502	523

The faster rotational relaxation with the shorter rotational time constant τ_f is described as the motion of a restricted rotor (probe) having its transition dipole moment undergoing orientational diffusion within a semicone of angle θ_w about an imaginary axis. Thus, the faster and slower rotational time constants can be written as

$$\frac{1}{\tau_s} = \frac{1}{\tau_L} + \frac{1}{\tau_M} \quad (10)$$

$$\frac{1}{\tau_f} = \frac{1}{\tau_w} + \frac{1}{\tau_s} \quad (11)$$

TABLE 2: Fitted Fluorescence Transients of Acridine Orange in Various Environments

systems	wavelength (nm)	τ_1 (ns)	τ_2 (ns)	τ_3 (ns)
water (pH = 6.9)	532	0.46 (10.5%)	1.85 (89.5%)	
NaOH (pH = 13.6)	550	0.28 (26.4%)	1.46 (31.1%)	6.20 (42.5%)
RMs with water ($w_0 = 2.5$)	550	0.38 (11.4%)	2.78 (72.9%)	5.12 (15.7%)
RMs with water ($w_0 = 10.0$)	550	0.29 (8.9%)	2.19 (77.4%)	3.97 (13.7%)
RMs with NaOH ($w_0 = 2.5$)	470	0.12 (44.4%)	0.77 (21.7%)	2.77 (23.8%)
	530	0.28 (36.5%)	2.39 (41.7%)	9.21 (21.8%)
RMs with NaOH ($w_0 = 10.0$)	480	0.19 (46.6%)	2.06 (31.3%)	6.44 (22.1%)
	540	0.31 (26.2%)	2.79 (51.0%)	8.00 (22.8%)
20 mM CTAB	536	0.77 (23.6%)	1.65 (74.3%)	9.53 (2.1%)
50 mM SDS	530	0.23 (5%)	3.08 (90%)	5.51 (5%)
10 mM TX100	532	0.35 (7.8%)	2.20 (88.5%)	5.66 (3.7%)
SS-DNA	530		3.09 (23.3%)	5.38 (76.7%)
(GCGCGCGCGCGC) ₂ (oligo1)	530	1.62 (19.6%)	4.76 (80.4%)	
(CGCAAATTTGCG) ₂ (oligo2)	530	2.33 (32.1%)	5.15 (67.9%)	

TABLE 3: Solvation Correlation Data for AO in Various Environments

systems	blue/red end	τ_1 (ns)	τ_2 (ns)
RMs with water ($w_0 = 2.5$)		0.40 (48.5%)	3.65 (51.5%)
RMs with water ($w_0 = 10.0$)		0.55 (43.0%)	3.30 (57.0%)
RMs with NaOH ($w_0 = 2.5$)	NP1	0.30 (70.3%)	8.00 (29.7%)
	NP2	0.40 (49.7%)	2.55 (50.3%)
RMs with NaOH ($w_0 = 10.0$)	NP1	0.25 (63.4%)	1.70 (36.6%)
	NP2	0.10 (60.8%)	1.10 (39.2%)
50 mM SDS		0.55 (32.8%)	1.65 (67.2%)

τ_M , i.e., the rotational time constant for overall micellar tumbling can be obtained using the Stokes–Debye–Einstein relation,⁷⁶

$$\tau_M = \frac{4\pi\eta r_H^3}{3k_B T} \quad (12)$$

where η is the viscosity of the dispersant (solvent), r_H the hydrodynamic radius of the micelle, k_B the Boltzmann constant, and T the absolute temperature. The lateral diffusion coefficient⁷⁷ is defined as

$$D_L = \frac{r_M^2}{6\tau_L} \quad (13)$$

where r_M is the radius of spherical surface of micelle along which the probe translates.

According to this model, the rotational anisotropy decay function is denoted as

$$r(t) = r_0[\beta + (1 - \beta)e^{-t/\tau_1}]e^{-t/\tau_2} \quad (14)$$

Again, $\beta = S^2$, where S^2 is the generalized order parameter that describes the degree of restriction on the wobbling-in-cone orientational motion. S^2 satisfies the inequality $0 \leq S^2 \leq 1$, where $S^2 = 0$ describes unrestricted reorientation and $S^2 = 1$ means no wobbling-in-cone orientational motion. The semicone angle θ_w is obtained from the ordered parameter as follows:

$$S^2 = \left[\frac{1}{2}(\cos \theta_w)(1 + \cos \theta_w) \right]^2 \quad (15)$$

For $\theta_w \leq 30^\circ$, the wobbling-in-cone diffusion constant D_w is given by

$$D_w \cong 7\theta_w^2/24\tau_w \quad (16)$$

with θ in radians. However, for $\theta_w \geq 30^\circ$ and all θ_w , the D_w is given by

$$D_w = \frac{1}{[(1 - S^2)\tau_w]} \left[\frac{x^2(1+x)^2}{2(x-1)} \left\{ \ln\left(\frac{1+x}{2}\right) + \frac{(1-x)}{2} \right\} + \frac{(1-x)}{24}(6 + 8x - x^2 - 12x^3 - 7x^4) \right] \quad (17)$$

where $x = \cos \theta_w$, when $\theta_w = 180^\circ$, i.e., when there is no restriction to orientation, $S^2 = 0$, and $D_w = 1/6\tau_w$. Cases where the $r(t)$ of fluorescent probes attached to macromolecules does not decay to zero but to a finite value (r_∞) at longer times indicates that the macromolecular reorientation time is much longer than the fluorescence lifetime of the attached fluorophore and the fluorophore is not able to sample through all possible orientations.⁷⁸ In these cases, the difference ($r_0 - r_\infty$) has been used to extract the dynamical parameters. For micelles, the radius along which the probe moves is taken from ref 77 and for the RM from ref 16. The hydrodynamic radii of the micellar aggregates were, however, determined from our DLS instrument.

Results and Discussion

Figure 1a shows the absorption spectra of AO in water (pH = 6.9) and RMs containing water. The absorption spectra show a slight red shift from 492 nm in water to 495 nm in AOT RMs, which indicates a finite interaction between AO and RM. The shoulder at 467 nm in the absorption spectrum of AO in water is due to the formation of dimeric AO in water.⁴⁵ It is known that AO is more sensitive to polarizability of environment than the polarity.⁵¹ The red shift may indicate the location of AO closer to the RM interface with higher polarizability than the central water core of the RM. Also, in $w_0 = 2.5$, the FWHM of the absorption spectrum is higher than that in water, indicative of AO being present in a heterogeneous environment. However, in $w_0 = 10$ RMs, the FWHM is close to that of water, which may indicate that AO molecules are a little away from the interface toward core water than in $w_0 = 2.5$ RMs. This may seem obvious because the diameter of the $w_0 = 2.5$ RM water pool is ~ 10 Å and the diameter of AO is 6.9 Å⁷⁹; thus, AO is much closer to the interface in $w_0 = 2.5$ RM.

Figure 2a shows the fluorescence spectra of AO in water and RMs containing water. The fluorescence maximum of AO in water is at 532 nm; that in $w_0 = 2.5$ and 10 RMs are at 549 and 545 nm, respectively. The slight blue shift of the fluorescence maximum of AO in $w_0 = 10$ compared with that in $w_0 = 2.5$ once again proves the location of AO to be slightly away from the RM interface toward core water in $w_0 = 10$ RMs compared with $w_0 = 2.5$ RMs. Figures 1b and 2b show the absorption

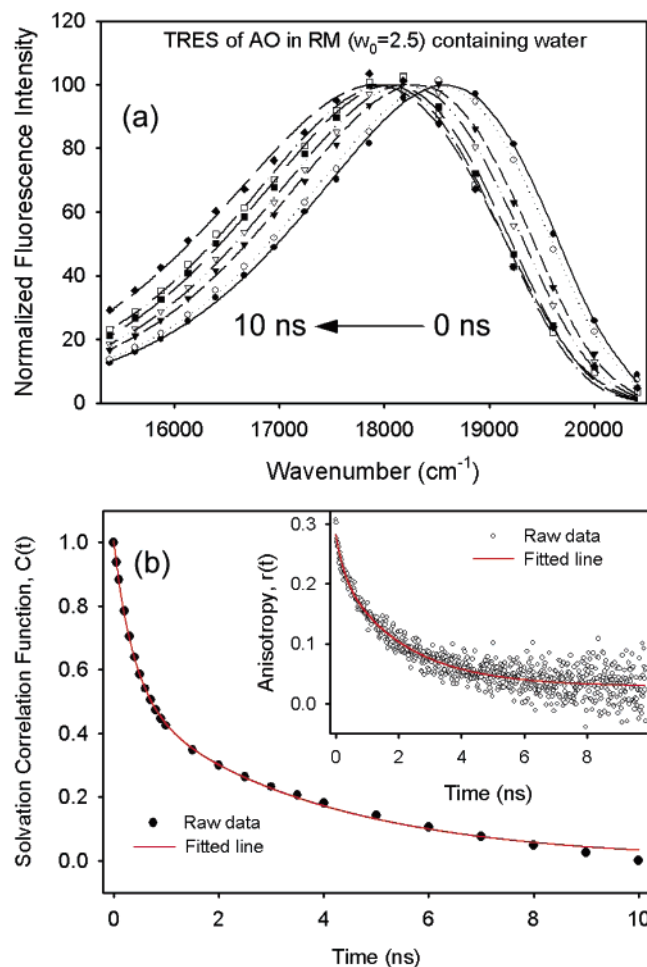


Figure 4. (a) Time-resolved emission spectra (TRES) of AO in RMs ($w_0 = 2.5$) containing water, (b) solvation correlation curve, and temporal anisotropy decay curve (insert) of AO in RMs ($w_0 = 2.5$) containing water.

and emission spectra of AO in NaOH (pH = 13.6) and that in RM containing NaOH. AO in NaOH solution has an absorption peak at 435 nm; the emission maximum is at 546 nm. These peaks correspond to that of deprotonated basic acridine orange (Scheme 1).⁴⁵ However, in RMs containing NaOH of $w_0 = 2.5$ and 10, a peak at 375 nm with a shoulder at 460 nm in the absorption spectra and a peak at ~ 535 nm with a shoulder at ~ 470 nm in the emission spectra are observed. These two peaks in the absorption and emission spectra indicate the existence of two types of AO: (i) basic AO in the nonpolar isooctane phase (absorption peak = 375 nm and emission peak = 470 nm) and (ii) protonated AO lying at the RM interface (absorption peak = 460 nm). The peaks at 533 ($w_0 = 2.5$) and 538 nm ($w_0 = 10$) could be due to formation of AO protonated at terminal amino groups⁴⁵ and/or an intracyclic imino group.

Figures 1c and 2c show the absorption and emission spectra of AO in 50 mM SDS (anionic), 20 mM CTAB (cationic), and 10 mM TX100 (neutral) surfactant solutions and that in genomic salmon sperm DNA and two synthetic DNA oligomers—oligo1 and oligo2. In all the micelles, the absorption and emission spectra indicate AO to be present in the stern layer of the micelles (Table 1). However, in both genomic and synthetic DNA, the absorption and emission spectra are 10 nm red-shifted and 6 nm blue-shifted, respectively, compared with that of AO in water, indicating AO to be intercalated inside the DNA.^{51,62} The absorption and fluorescence peaks of AO in various environments are given in Table 1.

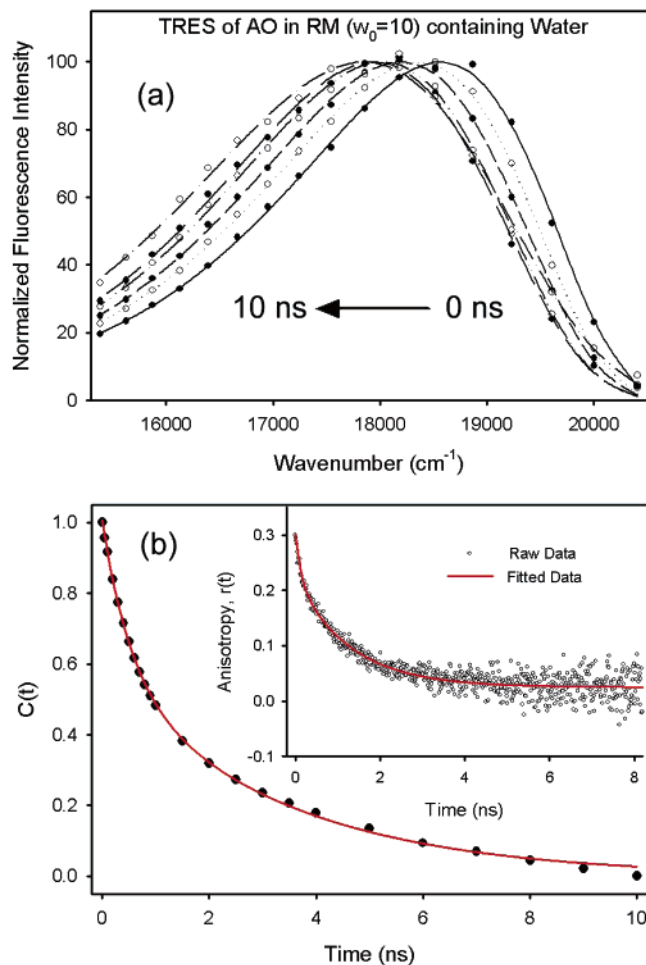


Figure 5. (a) Time-resolved emission spectra (TRES) of AO in RMs ($w_0 = 10$) containing water, (b) solvation correlation curve, and temporal anisotropy decay curve (insert) of AO in RM ($w_0 = 10$) containing water.

Figure 3a,b shows the fluorescence decay transients of AO in RMs ($w_0 = 2.5$) containing water and that containing NaOH at various wavelengths. In the case of RMs containing water, the fluorescence transients are found to decay at blue wavelengths and a corresponding rise is seen at red wavelengths. This observation is consistent with the clear case of solvation of AO within the RM⁶⁸ (see below). However, in the case of RMs containing NaOH, only decay components are observed at all wavelengths with comparatively longer components at higher wavelengths. This observation may indicate the presence of more than one species, which may or may not be kinetically coupled in the excited or ground state, or a single species having more than one type of environment. The fitted fluorescence decay data of AO under various conditions are given in Table 2. Figures 4a and 5a show the time-resolved emission spectra (TRES) of AO in RMs containing water of $w_0 = 2.5$ and 10, respectively. The constructed solvation correlation function (Figures 4b and 5b) with solvation shifts 671 ($w_0 = 2.5$) and 711 cm^{-1} ($w_0 = 10$) shows a biexponential decay. The solvation time constants are given in Table 3. The similarity of both the faster and slower time constants indicates the presence of AO in similar environments near the interface in both the RMs. The faster and slower time constants correspond to solvation by free water (core type) and bound water (interfacial type), respectively. It has to be noted that the TRANES of AO (data not shown) in the RMs containing water do not exhibit any

TABLE 4: Temporal Fluorescence Anisotropy Decay Data for Acridine Orange in Various Environments

systems	wavelength (nm)	ϕ_1 (ns)	ϕ_2 (ns)	r_0	r_∞
water (pH = 6.9)	532	0.11 (100.00)	—	0.359	0.00
NaOH (pH = 13.6)	550	0.14 (100.00)	—	0.336	0.00
RMs with water ($w_0 = 2.5$)	550	0.27 (20.53)	2.10 (79.47)	0.254	0.014
RMs with water ($w_0 = 10.0$)	550	0.16 (25.84)	1.31 (74.16)	0.266	0.010
RMs with NaOH ($w_0 = 2.5$)	470	0.20 (33.35)	3.20 (66.65)	0.249	0.003
	530	0.22 (18.65)	2.74 (81.35)	0.209	0.006
RMs with NaOH ($w_0 = 10.0$)	480	0.19 (46.77)	1.20 (53.23)	0.241	0.012
	540	0.28 (34.82)	2.23 (65.18)	0.226	0.013
20 mM CTAB	536	0.09 (68.30)	0.90 (31.70)	0.243	0.002
50 mM SDS	530	0.12 (60.02)	1.12 (39.98)	0.364	0.001
10 mM TX100	532	0.30 (44.22)	2.49 (55.78)	0.194	0.000
SS-DNA	530	0.13 (53.39)	5.52 (46.61)	0.212	0.095
(GCGCGCGCGC) ₂ (oligo1)	530	0.08 (33.52)	2.08 (66.48)	0.182	0.000
(CGCAAATTTGCG) ₂ (oligo2)	530	0.36 (16.76)	2.18 (83.24)	0.173	0.000

TABLE 5: Wobbling-in-Cone Data of Acridine Orange in Various Environments

systems	τ_f (ns)	τ_r (ns)	S^2	θ (deg)	τ_M (ns)	τ_L (ns)	τ_w (ns)	$D_M \times 10^{-6}$ (s ⁻¹)	$D_w \times 10^{-8}$ (s ⁻¹)	$D_L \times 10^6$ (cm ² s ⁻¹)
RMs with water ($w_0 = 2.5$)	0.27	2.10	0.7947	22.21	2.40	16.80	0.309	69.44	1.42	0.05
RMs with water ($w_0 = 10$)	0.16	1.31	0.7416	25.26	22.39	1.39	0.181	7.44	3.13	4.36
RMs with NaOH ($w_0 = 2.5$) 470 nm	0.20	3.20	0.6665	29.29	2.09		0.216	79.74	3.54	
RMs with NaOH ($w_0 = 2.5$) 535 nm	0.22	2.74	0.8135	21.07	2.09		0.234	79.74	1.68	
RMs with NaOH ($w_0 = 10$) 470 nm	0.19	1.99	0.5323	36.16	13.64	2.32	0.208	12.22	5.59	5.56
RMs with NaOH ($w_0 = 10$) 538 nm	0.28	2.23	0.6518	30.06	13.64	2.67	0.318	12.22	2.52	4.17
20 mM CTAB 536 nm	0.09	0.90	0.3170	47.70	27.37	0.93	0.104	6.09	19.50	8.43
50 mM SDS 530 nm	0.12	1.12	0.3998	43.06	8.64	1.29	0.133	19.29	12.38	3.60
10 mM TX100 532 nm	0.30	2.49	0.5578	34.87	96.86	2.56	0.338	1.72	3.19	12.05
SS-DNA	0.13	5.52	0.4661	39.56			0.135		10.28	
oligo1	0.08	2.08	0.6648	29.38			0.084		9.10	
oligo2	0.36	2.18	0.8324	19.88			0.427		0.82	

isoemissive point, indicating that the dynamics of solvation of the probe in the RMs are essentially due to a single species.

Inserts of Figures 4b and 5b show the temporal anisotropy decay $r(t)$ of AO in $w_0 = 2.5$ and 10 RMs containing water. The rotational correlation time constants are given in Table 4. It is found that both the slower and faster anisotropy time constants have decreased for AO in RMs ($w_0 = 10$) compared with that in $w_0 = 2.5$ RM. This is an indication of the fact that, in larger RMs, AO is much freer to move. The wobbling-in-cone model analysis of the $r(t)$ data shows that the semicone angle inscribed by AO in smaller RMs is 22.21° and that in the larger one is 25.26° (from eq 15). Also, the diffusion constant of lateral diffusion of AO in smaller RMs ($w_0 = 2.5$) is 2 orders of magnitude lower than that in the larger one ($w_0 = 10$). The rotational time constants and diffusion coefficients for overall micellar motion, lateral diffusion of AO along the interface, and wobbling-in-cone motion of AO are given in Table 5. The lateral diffusion time constant of 16.8 ns in $w_0 = 2.5$ RMs shows that there is no appreciable translation of AO within its lifetime in this small RM.

Figures 6a and 7a show the TRANES of AO in RMs of $w_0 = 2.5$ and 10 containing NaOH, respectively. In both the spectra, an isoemissive point is observed (503 nm for $w_0 = 2.5$ and 514 nm for $w_0 = 10$ RMs). In both the cases, the intersection points lie in between the emission maxima of basic AO in the isooctane phase and that of protonated AO at the RM interface. Thus, RMs containing NaOH have two types of AO: basic and protonated AO. Although RMs containing NaOH have a pH of 13.6, which is higher than the excited pK_a ($= 13.3$) of basic AO,⁴⁵ the signature of protonated AO is found because it is known that the pH at the interface of anionic micelles or reverse micelles are less than that of the bulk water or free water at the center of the RM.^{80,81} Because RMs containing NaOH have two types of AO in two different environments, the TRES of AO in these RMs ($w_0 = 2.5$ and 10) showed two peaks correspond-

ing to two different types of AO molecules from the time zero itself (data not shown). As a result, the TRES of AO in these RMs could not be fitted with a single log-normal function but with a double log-normal one. We have followed the peak shift of these two peaks one at red end (NP1) and the other at the blue end (NP2) with time to determine the solvation relaxation time scales of these two different AO molecules. Similar spectral deconvolution is reported in the recent literature.⁸²

Figure 6b shows the temporal peak shift at red wavelength NP1 (for protonated AO at the interface) and blue wavelength NP2 (for basic AO in the isooctane phase) (insert of Figure 6b) derived from the TRES of AO in RMs ($w_0 = 2.5$) containing NaOH. The shorter time constants are the same at both wavelengths, indicating long-range dipolar relaxation due to reorganization of core-type water molecules; longer time constants correspond to relaxation by interfacial water (2.55 ns) of protonated AO and deep trap water (8 ns) of basic AO in the nonpolar phase. Similarly, Figure 7b shows the temporal peak shift of AO in the nonpolar isooctane phase and interface in $w_0 = 10$ RMs containing NaOH. The longer time constant of 8 ns is not observed here because, in larger RMs, AOT monomers are properly arranged in a monolayer about the aqueous pool¹⁶ and the number of deep trap water may be too sparse to contribute to the relaxation. In this case also, a biexponential decay is observed, indicating solvation by free water and bound interfacial water. Figures 6c and 7c show the fluorescence anisotropy decay of AO in RMs ($w_0 = 2.5$ and 10) containing NaOH. In both cases, the decay is found to be biexponential (Table 4). From wobbling-in-cone model analysis (Table 5), the semicone angle for AO in the isooctane phase is found to be larger than at the interface, indicating greater restriction at the interface. The time constants and diffusion coefficients for wobbling, lateral motion of AO, and overall macromolecular motion in various environments are tabulated in Table 5. However, in $w_0 = 2.5$ RMs containing NaOH, the

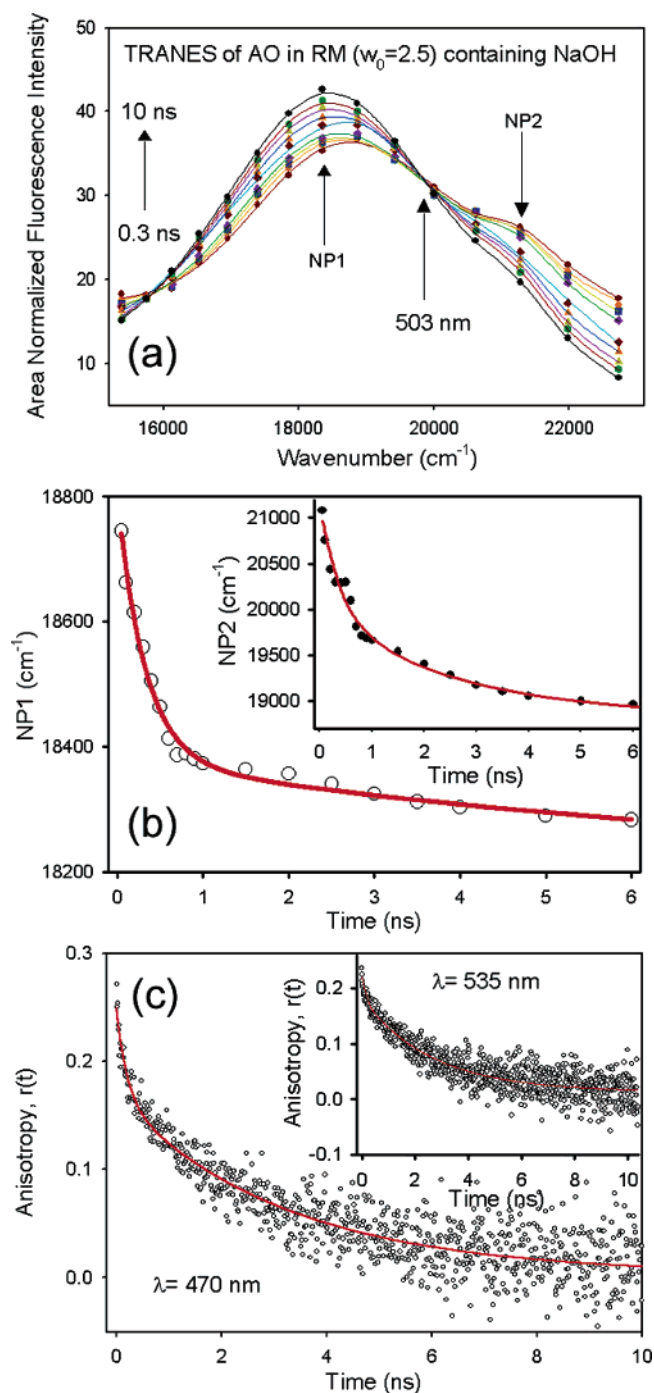


Figure 6. (a) Time-resolved area normalized emission spectra (TRES) of AO in RMs ($w_0 = 2.5$) containing NaOH, (b) temporal peak shift at red wavelength (NP1) and blue wavelength (NP2) (insert), and (c) temporal anisotropy decay curve at 470 and 535 nm (insert) of AO in RMs ($w_0 = 2.5$) containing water.

translation diffusion time constant is found to be negative for both types of AO, which indicates that the lateral diffusion time constant for the particular case cannot be extracted from eq 10 and appeals further investigation.

In order to compare the solvation and rotational dynamics of AO in RMs with that in normal micelles, we have studied the AO in 50 mM SDS (anionic), 20 mM CTAB (cationic), and 10 mM TX100 (neutral) micelles. Figure 8a shows the TRANES of AO in 50 mM SDS; an isoemissive point is observed at 530 nm. It is known that AO interacts with SDS micelles through both hydrophobic and electrostatic interactions. Thus, the hydrophobic aromatic rings of the AO molecule remain within

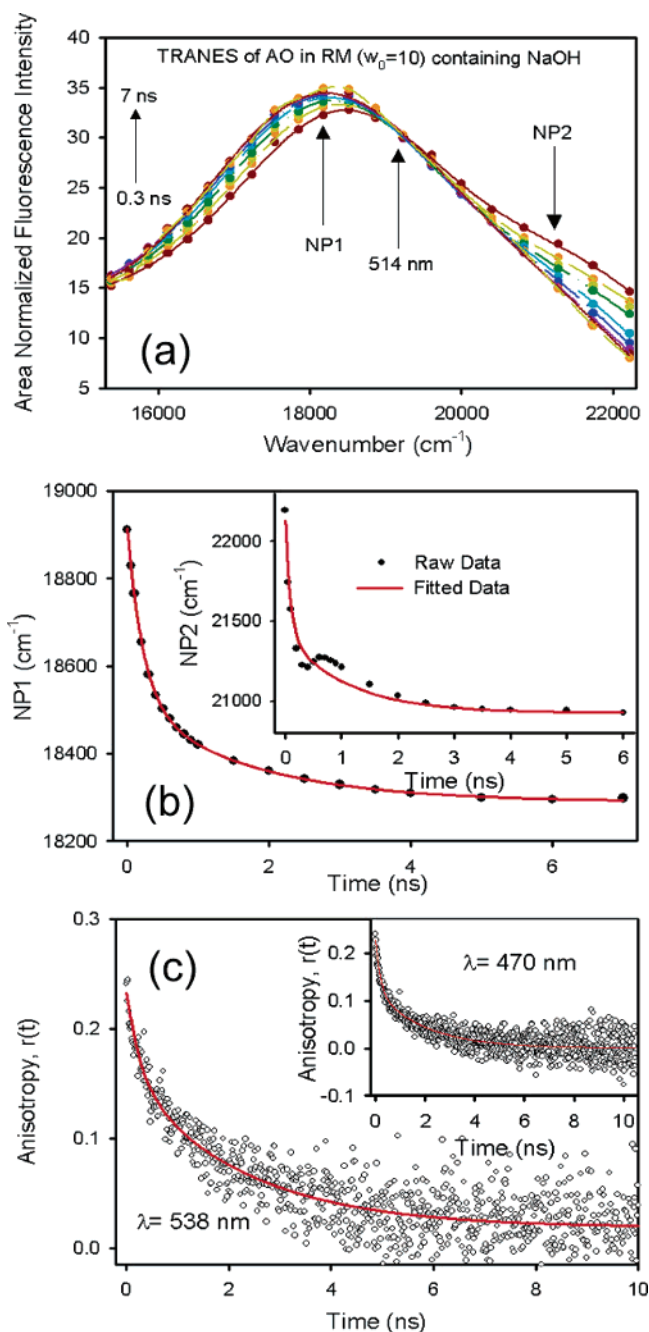


Figure 7. (a) Time-resolved area normalized emission spectra (TRES) of AO in RMs ($w_0 = 10$) containing NaOH, (b) temporal peak shift at red wavelength (NP1) and blue wavelength (NP2) (insert), and (c) temporal anisotropy decay curve at 538 and 470 nm (insert) of AO in RMs ($w_0 = 10$) containing water.

the hydrophobic core of the SDS micelle, and the charged intracyclic imino group and the two terminal polar amino groups remain outward directed toward the stern layer.^{83–85} This in turn results in an isoemissive point at 530 nm. The solvation correlation curve of AO in SDS (Figure 8b, insert) is biexponential in nature with a faster time constant (550 ps) due to reorganization of bulk type water molecules and a slower time constant (1.65 ns) due to reorganization of bound water in the stern layer. It is observed that the slower time constant in SDS micelle is smaller than that in RMs, which may indicate that bound water is much more rigid in RMs than in normal micelles. Figure 8b shows the temporal anisotropy decay of AO in 50 mM SDS, 20 mM CTAB, and 10 mM TX100 micelles. In all these micelles, biexponential decay of temporal anisotropy

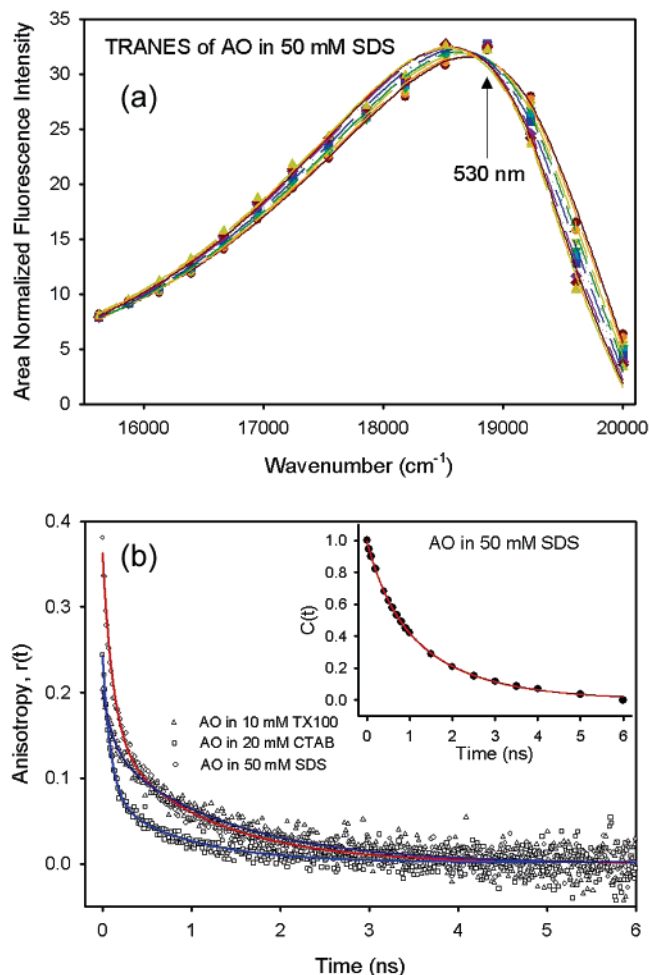


Figure 8. (a) Time-resolved area normalized emission spectra (TRES) of AO in 50 mM SDS solution and (b) temporal anisotropy decay curve of AO in 10 mM TX100, 20 mM CTAB, and 50 mM SDS solutions and solvation correlation curve of AO in 50 mM SDS solution (insert).

decays are observed (Table 4). Both the faster and slower rotational time constants of AO in CTAB micelles are much faster than in other micelles. This is due to the fact that AO being cationic in nature is away from the positively charged micellar surface. However, the possibility of a hydrophobic interaction of AO with this micelle may not be completely ruled out.⁸⁵ Hence, due to hydrophobic interactions, AO remains partly in the stern layer of CTAB micelles with a major portion of AO in bulk water. Because in this case AO is more in bulk type water, solvation is much faster. The time scale of this solvation is faster than our instrumental resolution and could not be detected. This is supported by the similarity of fluorescence decay at all wavelengths. In case of AO in CTAB, because AO is least restricted, the highest semicone angle (47.7°) and lateral diffusion coefficient ($8.43 \times 10^{-6} \text{ cm}^2 \text{ s}^{-1}$) are exhibited, indicating faster lateral diffusion. The interaction of AO with neutral TX100 micelles is mainly hydrophilic in nature.⁴⁴ AO and water molecules compete for hydrating the polyoxyethylene head group of TX100 micelles. So, AO is located preferentially in the hydration zone of the oxyethylene chains. The two rotational correlation time constants of 300 ps and 2.49 ns (Table 4) are slower than that in other micelles, indicating greater restriction on the wobbling motion ($\tau_w = 338$ ps) and lateral diffusion ($\tau_L = 2.56$ ns) of AO in TX100 micelles. However, the lateral diffusion coefficient appears to be larger in TX100 than that in other micelles despite the higher τ_L . This is due to the large size of the TX100 micelle revealing larger D_L values

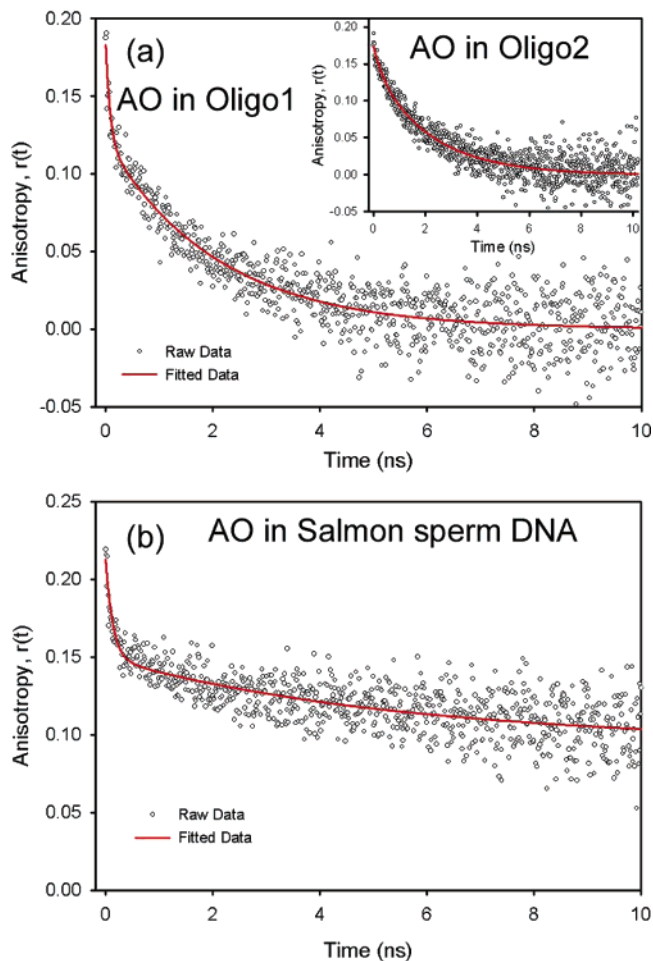


Figure 9. Temporal anisotropy decay curves of AO in (a) oligo1 and oligo2 (insert) and (b) salmon sperm DNA.

from eq 13. In all the cases of micelles, the r_0 values and wobbling-in-cone data are tabulated in Table 5. In the case of TX100 micelles also, there is no appreciable difference in temporal decay transients at blue and red wavelengths depicting a faster solvation shift with time scales faster than our instrumental resolution.

The bending and flexing motions of DNA along with the internal motions are very important for chemical reactions taking place at a given site of DNA and for the process of DNA condensation.^{63,86–88} Hence, knowing the time scales of internal motions in DNA gives a complete physical picture of DNA. The relaxation dynamics of DNA environments^{51,89–91} and water molecules in the close vicinity of the minor groove of genomic and synthesized DNAs^{92,93} have been explored by using time-dependent Stokes shift methods. Fluorescence polarization techniques, utilizing ethidium bromide (EB) as an intercalator, have been extensively used to study the internal and overall motions in DNA.^{94–97} Both steady state⁹⁸ and time-resolved^{94–97,99} measurements of temporal fluorescence anisotropy have been used to examine motions with correlation times ranging from 0.1 to more than 100 ns. Barkley and Zimm⁸⁸ in their elastic continuum model of DNA predicted that fluorescence polarization anisotropy of an intercalated dye is complex containing exponentials in $t^{1/2}$ due to torsion (twisting) and in $t^{1/4}$ due to bending motions, which is equivalent to the bead spring model developed by Allison and Schurr¹⁰⁰ and LeBret.⁸⁶ In the bead-spring model, in addition to twisting motion at intermediate times, initial exponential decay characteristics of uncoupled motions of individual beads at short times were observed. It

has been found by Millar et al. that torsional rigidity of different varieties of DNA are different and initial loss in anisotropy is either due to rapid internal motion of the double helix or independent motion of the dye.⁹⁵ For an intercalating dye within DNA, there is no water and the entire dynamics is essentially controlled by the electric field of DNA. To study the wobbling motion of the polynuclear heteroaromatic dye AO in the DNAs we have applied the wobbling-in-cone model to the temporal anisotropy of the intercalated dye. We have prepared complexes of AO with genomic salmon sperm DNA (40% GC content¹⁰¹) and two synthetic DNA dodecamers—oligo1 and oligo2. Although binding of AO to DNA is sequence-independent, slight preferential binding of AO to GC base pairs has been noted.¹⁰² In all the three AO–DNA complexes, the structural integrity of the DNA was restored as confirmed through CD study (data not shown). Figure 9a shows the temporal anisotropy decay of AO intercalated to oligo1 and oligo2. The anisotropy data are tabulated in Table 4.

Figure 9b shows the temporal anisotropy decay of AO complexed with SS-DNA. It is found that the $r(t)$ decays to zero within 10 ns for the dodecamers and there remains an offset (r_∞) of 0.095 for SS-DNA. This fact indicates that the large genomic DNA executing end-over-end rotations does not rotate appreciably within the fluorescence lifetime of the intercalator AO. From Figure 9, it is also observed that the temporal anisotropy decay is readily fit into biexponential decay for all the DNAs. From Table 4, the faster rotational time constant for AO in oligo1 is about 4 times lesser than that in oligo2. This could be due to charge transfer between AO and GC base pairs flanking the intercalated AO in oligo1,^{48,99,103} which is hindered in oligo2 and SS-DNA (mixed polymers of AT and GC base pairs). This is also reflected in the faster fluorescence decay of AO in oligo1 compared to oligo2 (see Table 2). The slower rotational time constants are however the same for both the DNA oligomers, which may be due to similarity of length and volumes of the two oligomers. The slower anisotropy time constant of 5.518 ns in SS-DNA may be due to the local tumbling of DNA segments. In this case, we cannot expect lateral diffusion of AO along the DNA–water interface as at [AO]:[DNA] = 1:100 all the AO molecules are intercalated to DNA.⁵⁰ From Table 5, it is observed that the semicone angle inscribed by the wobbling AO is in the order SS-DNA > oligo1 > oligo2. Comparison of the two synthetic DNA indicates that AO is much more free to wobble in the GC site than in the AT binding site, and/or the GC-rich DNA (oligo1) is less rigid than the dodecamer containing both AT and GC base pairs. However, in SS-DNA, it is still larger, which may be due to the twisting motion of the DNA chain combining with the internal wobbling of the dye to produce a larger semicone angle. Here, we find that the semicone angle inscribed by the restricted motion of AO in the intercalation site is larger than that inscribed by EB (15°).⁹⁴ This may be due to the fact that AO suffers less hindrance compared to EB because of the absence of a phenyl group and possible hydrogen bonding between amino protons of EB and the DNA phosphate backbone.⁹⁷ Another interesting factor to note is that the generalized order parameters for synthetic oligonucleotides are larger than that for the genomic DNA, which indicate that the smaller DNA are much more rigid than larger genomic DNA providing greater restriction to the internal wobbling motion of the dye.

Conclusion

This study provides a detailed picture of dynamics and location of acridine orange in biomimetics (micelles and reverse

micelles) and in DNA. The equivalent nature of solvation correlation curve of AO in $w_0 = 2.5$ and 10 RMs containing water indicates almost similar environments (i.e., interface) around AO in RMs. In RMs containing NaOH, the presence of an isoemissive point indicates the existence of two types of AO: basic AO in the isoctane phase and protonated AO at the interface. Despite the pH of NaOH being higher than the excited state pKa (13.3) of AO, protonated AO is observed at the interface, which indicates that the interfacial pH is lower than the pH at the core. The lower value of the longer solvation correlation time constant for AO in SDS compared to that in RMs indicates that the bound water in RMs is much more rigid than that in normal SDS micelles. Wobbling-in-cone data analysis indicates that AO wobbles much more freely in larger RMs inscribing larger semicone angles. Among the micelles, the largest semicone angle is exhibited in the CTAB micelle, which is due to repulsion between cationic AO and positively charged head groups of CTAB micelles that pushes AO away from the micellar surface. The generalized order parameter for AO in genomic salmon sperm DNA is lower than that in synthetic DNA, which indicates that AO intercalated to synthetic DNA experiences much more restriction. Again, comparison of two synthetic DNAs (oligo1 and oligo2) indicates that AT containing synthetic DNA (oligo2) is much more rigid than GC-rich DNA (oligo1) as indicated by the S^2 and semicone angle values. Also, comparison with previous studies on DNA shows that AO is much freer to wobble in its intercalation site than EB. Finally, this study would prove to be very useful for predicting mechanisms of reactions involving acridine orange in biomimetics and DNA.

Acknowledgment. A. K. S. thanks UGC for fellowship. We thank DST for a financial grant (SR/FTP/PS-05/2004).

References and Notes

- (1) Sepulveda, L.; Lissi, E.; Quina, F. *Adv. Colloid Interface Sci.* **1986**, *25*, 1–57.
- (2) Abrahams, M. H.; Chadha, H. S.; Dixon, J. P.; Ryol, C. *J. Chem. Soc., Perkin Trans.* **1995**, *2*, 887–894.
- (3) Abuin, E.; Lissi, E. *Bol. Soc. Chile Quim.* **1997**, *42*, 113.
- (4) Luisi, P. L.; Giomini, M.; Pileni, M. P.; Robinson, B. H. *Biochim. Biophys. Acta* **1988**, *947*, 209–246.
- (5) Fendler, J. H. *Acc. Chem. Res.* **1976**, *9*, 153–161.
- (6) De, T. K.; Maitra, A. *Adv. Colloid Interface Sci.* **1995**, *59*, 95–193.
- (7) Bhattacharya, K.; Bagchi, B. *Chem. Rev.* **2000**, *100*, 2046.
- (8) Bhattacharyya, K. *Acc. Chem. Res.* **2003**, *36*, 95–101.
- (9) Bhattacharyya, K.; Bagchi, B. *J. Phys. Chem. A* **2000**, *104*, 10603–10613.
- (10) Cohen, B. E.; Huppert, D.; Solntsev, K. M.; Tsfadia, Y.; Nachiel, E.; Gutman, M. *J. Am. Chem. Soc.* **2002**, *124*, 7539–7547.
- (11) Kalyanasundaram, K. In *Photochemistry in microheterogeneous systems*; Academic press: New York, 1987.
- (12) Pileni, M. P. *Adv. Colloid Interface Sci.* **1993**, *46*, 139–163.
- (13) Carvalho, C. M.; Cabral, J. M. *Biochimie* **2000**, *82*, 1063–1085.
- (14) Fendler, J. H.; Fendler, E. J.; Medary, R. T.; Woods, V. A. *J. Am. Chem. Soc.* **1972**, *94*, 7288–7295.
- (15) El Seoud, O. A.; Fendler, E. J.; Fendler, J. H. *J. Chem. Soc., Faraday Trans. 1* **1974**, *70*, 459–470.
- (16) Maitra, A. *J. Phys. Chem.* **1984**, *88*, 5122–5125.
- (17) Jain, T. K.; Varshney, M.; Maitra, A. *J. Phys. Chem.* **1989**, *93*, 7409–7416.
- (18) Tan, H. S.; Piletic, I. R.; Fayer, M. D. *J. Chem. Phys.* **2005**, *122*, 175011–175019.
- (19) Piletic, I. R.; Moilanen, D.; Spry, D. B.; Levinger, N. E.; Fayer, M. D. *J. Phys. Chem. A* **2006**, *110*, 4985–4999.
- (20) Piletic, I. R.; Moilanen, D.; Levinger, N. E.; Fayer, M. D. *J. Am. Chem. Soc.* **2006**, *128*, 10366–10367.
- (21) Hu, M.; Kevan, L. *J. Phys. Chem.* **1979**, *94*, 5348–5351.
- (22) Zulauf, M.; Eicke, H.-F. *J. Phys. Chem.* **1979**, *83*, 480–486.
- (23) Day, R. A.; Robinson, B. H.; Clarke, J. H.; Doherty, J. V. *J. Chem. Soc., Faraday Trans. 1* **1979**, *75*, 132–139.
- (24) Cabos, C.; Delord, P. *J. Phys. Lett.* **1980**, *41*, L-455.

- (25) Fletcher, P. D. I.; Robinson, B. H.; Tabony, J. *J. Chem. Soc., Faraday Trans. 1* **1986**, *82*, 2311–2321.
- (26) Angelo, M. D.; Floretto, D.; Onori, G.; Palmitori, L.; Santucci, A. *Phys. Rev. E* **1996**, *54*, 993–996.
- (27) Middleton, M. A.; Schetchter, R. S.; Johnston, K. P. *Langmuir* **1990**, *6*, 920–928.
- (28) Faeder, J.; Ladanyi, B. M. *J. Phys. Chem. B* **2005**, *109*, 6732–6740.
- (29) Brand, L.; Gohlke, J. R. *Annu. Rev. Biochem.* **1972**, *41*, 843–868.
- (30) Howe, A. M.; Toprakcioglu, C.; Dore, J. C.; Robinson, B. H. *J. Chem. Soc., Faraday Trans. 1* **1986**, *82*, 2411–2422.
- (31) Corbeil, E. M.; Riter, E. M.; Levinger, N. E. *J. Phys. Chem. B* **2004**, *108*, 10777–10784.
- (32) Levinger, N. E. *Curr. Opin. Colloid Interface Sci.* **2000**, *5*, 118–124.
- (33) Correa, N. M.; Levinger, N. E. *J. Phys. Chem. B* **2006**, *110*, 13050–13061.
- (34) Bardez, E.; Goguillon, B. T.; Keh, E.; Valeur, B. *J. Phys. Chem.* **1984**, *88*, 1909–1913.
- (35) Bardez, E.; Monnier, E.; Valeur, B. *J. Phys. Chem.* **1985**, *89*, 5031–5036.
- (36) Mandal, D.; Pal, S. K.; Sukul, D.; Bhattacharyya, K. *J. Phys. Chem. A* **1999**, *103*, 8156–8159.
- (37) Escabi-Perez, J. R.; Fendler, J. H. *J. Am. Chem. Soc.* **1978**, *100*, 2234–2236.
- (38) Kwon, O.-H.; Jang, D.-J. *J. Phys. Chem. B* **2005**, *109*, 20479–20484.
- (39) Giestas, L.; Yihwa, C.; Lima, J. C.; Vautier-Giongo, C.; Lopes, A.; Macanita, A. L.; Quina, F. H. *J. Phys. Chem. A* **2003**, *107*, 3263–3269.
- (40) Correa, N. M.; Biasutti, M. A.; Silber, J. J. *J. Colloid Interface Sci.* **1995**, *172*, 71–76.
- (41) Correa, N. M.; Biasutti, M. A.; Silber, J. J. *J. Colloid Interface Sci.* **1995**, *184*, 570–578.
- (42) Zhang, J.; Bright, F. V. *J. Phys. Chem.* **1991**, *95*, 7900–7907.
- (43) Pal, S. K.; Mandal, D.; Bhattacharyya, K. *J. Phys. Chem. B* **1998**, *102*, 11017–11023.
- (44) Andrade, S. M.; Costa, S. M. B. *Photochem. Photobiol. Sci.* **2002**, *1*, 500–506.
- (45) Falcone, R. D.; Correa, N. M.; Biasutti, M. A.; Silber, J. J. *Langmuir* **2002**, *18*, 2039–2047.
- (46) Pereira, R. V.; Gehlen, M. *Spectrochim. Acta, Part A* **2005**, *61*, 2926–2932.
- (47) Falcone, R. D.; Correa, N. M.; Biasutti, M. A.; Silber, J. J. *J. Colloid Interface Sci.* **2006**, *296*, 356–364.
- (48) Kononov, A. I. *J. Phys. Chem. B* **2001**, *105*, 535–541.
- (49) Lerman, L. S. *Proc. Natl. Acad. Sci. U.S.A.* **1963**, *49*, 94–102.
- (50) Lyles, M. B.; Cameron, I. L. *Biophys. Chem.* **2002**, *96*, 53–76.
- (51) Brauns, E. B.; Murphy, C. J.; Berg, M. A. *J. Am. Chem. Soc.* **1998**, *120*, 2449–2456.
- (52) Mosalenko, S. A.; Sinyak, V. A.; Shekun, Y.-G. *Phys. Lett.* **1982**, *110A*, 432–434.
- (53) Wainwright, M. *J. Antimicrob. Chemother.* **2001**, *47*, 1–13.
- (54) Blears, D. J.; Danyluk, S. S. *J. Am. Chem. Soc.* **1967**, *89*, 21–26.
- (55) Costantino, L.; Guarino, G.; Ortona, O.; Vitagliano, V. *J. Chem. Eng. Data* **1984**, *29*, 62–66.
- (56) Luchowski, R.; Krawczyk, S. *Chem. Phys.* **2003**, *293*, 155–166.
- (57) Petit, J.-M.; Gray, M. D.; Ratinaud, M.-H. *Biol. Cell.* **1993**, *78*, 1–13.
- (58) Chan, M. S.; Bolton, J. R. *Photochem. Photobiol.* **1981**, *34*, 537–547.
- (59) Schmidt, H.; Al-Ibrahim, A.; Dietzel, U. L. B. *Photochem. Photobiol.* **1981**, *33*, 127–130.
- (60) Chou, S.-H.; Wirth, M. J. *J. Phys. Chem.* **1989**, *93*, 7694–7698.
- (61) Wirth, M. J.; Burbage, J. D. *J. Phys. Chem.* **1992**, *96*, 9022–9025.
- (62) Shaw, A. K.; Sarkar, R.; Pal, S. K. *Chem. Phys. Lett.* **2005**, *408*, 366–370.
- (63) Maniatis, T.; Venable, J. J. H.; Lerman, L. S. *J. Mol. Biol.* **1974**, *88*, 37–56.
- (64) Cosa, G.; Focsaneanu, K.-S.; McLean, J. R. N.; McNamee, J. P.; Scaiano, J. C. *Photochem. Photobiol.* **2001**, *73*, 585–599.
- (65) Gallagher, S. R. In *Current Protocols in Molecular Biology*; Ausubel, F. M., Brent, R., Kingston, K. E., Moore, D. D., Seidman, J. G., Smith, J. A., Struhl, K., Eds.; Greene and Wiley-Interscience: New York, 1994; Vol. 28, Appendix 3D.
- (66) Horng, M. L.; Gardecki, J. A.; Papazyan, A.; Maroncelli, M. *J. Phys. Chem.* **1995**, *99*, 17311–17337.
- (67) Lakowicz, J. R. *Principles of fluorescence spectroscopy*; Kluwer Academic/Plenum: New York, 1999.
- (68) Periasamy, N.; Koti, A. S. R. *Proc. Indian Natl. Sci. Acad.* **2003**, *69A*, 41–48.
- (69) Koti, A. S. R.; Krishna, M. M. G.; Periasamy, N. *J. Phys. Chem. A* **2001**, *105*, 1767–1771.
- (70) Koti, A. S. R.; Periasamy, N. *Proc. Indian Natl. Sci. Acad. (Chem. Sci.)* **2001**, *113*, 157–163.
- (71) Chorvat, J., Jr.; Chorvatova, A. *Eur. Biophys. J.* **2006**, *36*, 73–83.
- (72) Novaira, M.; Biasutti, M. A.; Silber, J. J.; Correa, N. M. *J. Phys. Chem. B* **2007**, *111*, 748–759.
- (73) Lipari, G.; Szabo, A. *Biophys. J.* **1980**, *30*, 489.
- (74) Wang, C. C.; Pecora, R. J. *Chem. Phys.* **1980**, *72*, 5333.
- (75) Quitevis, E. L.; Marcus, A. H.; Fayer, M. D. *J. Phys. Chem.* **1993**, *97*, 5762–5769.
- (76) Debye, P. *Polar Molecules*; Dover: New York, 1929.
- (77) Maiti, N. C.; Krishna, M. M. G.; Britto, P. J.; Periasamy, N. *J. Phys. Chem. B* **1997**, *101*, 11051–11060.
- (78) Szabo, A. *J. Chem. Phys.* **1984**, *81*, 150–167.
- (79) Sharma, V. K.; Sahare, P. D.; Rastogi, R. C.; Ghoshal, S. K.; Mohan, D. *Spectrochim. Acta, Part A* **2003**, *59*, 1799–1804.
- (80) Mukerjee, P.; Banerjee, K. *J. Phys. Chem.* **1964**, *68*, 3567–3574.
- (81) Fujii, H.; Kawai, T.; Nishikawa, H.; Ebert, G. *Colloid Polym. Sci.* **1982**, *260*, 697–701.
- (82) Vincent, M.; de Foresta, B.; Gallay, J. *Biophys. J.* **2005**, *88*, 4337–4350.
- (83) Park, J. W.; Chung, H. *Bull. Korean. Chem. Soc.* **1986**, *7*, 113–116.
- (84) Wiosetek-Reske, A. M.; Wysocki, S. *Spectrochim. Acta, Part A* **2006**, *64*, 1118–1124.
- (85) Moulik, S. P.; Ghosh, S.; Das, A. R. *Colloid Polym. Sci.* **1979**, *257*, 645–655.
- (86) Le Bret, M. *Biopolymers* **1978**, *17*, 1939–1955.
- (87) Benham, C. J. *Biopolymers* **1979**, *18*, 609–623.
- (88) Barkley, M. D.; Zimm, B. H. *J. Chem. Phys.* **1979**, *70*, 2991–3007.
- (89) Brauns, E. B.; Madaras, M. L.; Coleman, R. S.; Murphy, C. J.; Berg, M. A. *J. Am. Chem. Soc.* **1999**, *121*, 11644–11649.
- (90) Brauns, E. B.; Madaras, M. L.; Coleman, R. S.; Murphy, C. J.; Berg, M. A. *Phys. Rev. Lett.* **2002**, *88*, 158101–158104.
- (91) Banerjee, D.; Pal, S. K. *Chem. Phys. Lett.* **2006**, *432*, 257–262.
- (92) Pal, S. K.; Zhao, L.; Zewail, A. H. *Proc. Natl. Acad. Sci. U.S.A.* **2003**, *100*, 8113–8118.
- (93) Pal, S. K.; Zhao, L.; Xia, T.; Zewail, A. H. *Proc. Natl. Acad. Sci. U.S.A.* **2003**, *100*, 13746–13751.
- (94) Millar, D. P.; Robbins, R. J.; Zewail, A. H. *Proc. Natl. Acad. Sci. U.S.A.* **1980**, *77*, 5593–5597.
- (95) Millar, D. P.; Robbins, R. J.; Zewail, A. H. *J. Chem. Phys.* **1982**, *76*, 2080–2094.
- (96) Magde, D.; Zappala, M.; Knox, M.; Nordlund, T. M. *J. Phys. Chem.* **1983**, *87*, 3286–3288.
- (97) Hard, T.; Kearns, D. *J. Phys. Chem.* **1986**, *90*, 3437–3444.
- (98) Genest, D.; Mirau, P. A.; Kearns, D. R. *Nucleic Acids Res.* **1985**, *13*, 2603–2615.
- (99) Hard, T.; Fan, P.; Magde, D.; Kearns, D. *J. Phys. Chem.* **1989**, *93*, 4338–4345.
- (100) Allison, S. A.; Schurr, J. M. *J. Chem. Phys.* **1979**, *41*, 35–59.
- (101) Chargaff, E.; Lipshitz, R.; Green, C.; Hodes, M. E. *J. Biol. Chem.* **1951**, *192*, 223–230.
- (102) Thomas, J. C.; Weill, G.; Daune, M. *Biopolymers* **1969**, *8*, 647–659.
- (103) Rayner, D. M.; Szabo, A. G.; Loutfy, R. O.; Yip, R. W. *J. Phys. Chem.* **1980**, *84*, 289–293.